

hinterland slope and geomorphic set up. In locations such as Kayamkulam, the hinterland regions have a downslope towards the backwaters. Thus it is quite possible that in many locations, the eroded sediments from the innershelf and the beach might have been carried forward and got deposited in the hinterland and backwater system, resulting in a localized temporary loss of sediment from the beach-innershelf region.

One aspect that has to be taken note of is the role of shore protection and other coastal engineering structures in tsunami inundation. The Kerala coast is notable for the presence of sea walls along a major part of it. Though well-built and well-maintained, sea walls were able to contain inundations in some locations, e.g. Thangassery, Neendakara, it failed in several other locations. Edavanakkad is a classical example where the sea wall, in spite of being well-built, was completely damaged with huge constituent boulders thrown far away inland. Thus, construction of sea walls as a protection against tsunami does not seem to have any apparent merit, considering also the exorbitant cost involved as well as the aesthetic and environmental considerations. On the other hand, coastal engineering structures seem to increase the vulnerability at least in some instances, as was seen near the Kayamkulam inlet. It could be argued that the inundation at Kayamkulam would have been much lower, but for the presence of the breakwaters jetting out into the sea and obstructing the northward propagation of the waves. Thus, there is no single way of reducing the effect of the tsunami and other coastal hazards; the varied morphology of our coastal regions and their socio-economic setting might call for adoption of region-specific strategies. Strict implementation of CRZ rules, adoption of soft coastal protection methods like beach nourishment, bio-shield, sand dune and development according to Integrated Coastal Zone Management Plan are strategies that could be followed for tsunami hazard mitigation<sup>12</sup>.

1. Narayana, A. C., Tatavarti, R. and Shakdwipe, M., Tsunami of 26 December 2004: Observations on Kerala coast. *J. Geol. Soc. India*, 2005, **65**, 239–246.
2. Berninghausen, W. H., Tsunamis and seismic seiches reported from regions adjacent to the Indian Ocean. *BSSA*, 1966, **56**, 1.
3. Wadia, D. N., *Geology of India*, Tata-McGraw Hill, New Delhi, 1981.
4. Preuss, P., Raad, P. and Bidoae, R., Mitigation strategies based on local tsunami effects. In *Tsunami Research at the End of a Critical Decade* (ed. Hebenstreit, G. T.), Kluwer, Dordrecht, 2001, pp. 47–64.
5. Website of International Tsunami Information Centre and other institutions.
6. Kurian, N. P. *et al.*, Heavy mineral budgeting and management at Chavara. Final Project Report, 2002, p. 513.
7. Black, K. P., *The 3DD Numerical Laboratory*, Assorted Software Manuals, Hamilton, New Zealand, 2001.
8. Mahadevan, R., Chandramohan, P. and Van Holland, G., Hydrodynamics of tsunami. Paper presented in the brainstorming session on tsunami mitigation strategies, Tiruchirappally, 25–26 February 2005.
9. Murthy, T. S. and Rao, A. D., The tsunami of 26th December 2004 in the Indian Ocean. Paper presented in the seminar on coastal protection, Thiruvananthapuram, 11 February 2005.

10. Bryant, E., *Tsunami, the Underrated Hazard*, Cambridge University, 2001, p. 320.
11. Chadha, R. K., Latha, G., Yeh, H., Peterson, C. and Katada, T., The tsunami of the Great Sumatra earthquake of  $M$  9.0 on 26 December 2004 – Impact on the east coast of India. *Curr. Sci.*, 2005, **88**, 1297–1301.
12. Baba, M. and Krishnan, K. R. S., Seminar on tsunami and coastal protection. *J. Geol. Soc. India*, 2005, **65**, 780–781.

ACKNOWLEDGEMENTS. We thank the ICMAM Project Directorate, Chennai for financial support. The Chief Hydrographer, Government of Kerala provided tide gauge data for Neendakara. We are grateful to Dr Kusala Rajendran for critical scrutiny of the manuscript and valuable suggestions. We also thank Dr M. Baba, Director, CESS, Thiruvananthapuram for support and encouragement provided.

Received 9 May 2005; revised accepted 7 October 2005

## Flood mapping and analysis using air-borne synthetic aperture radar: A case study of July 2004 flood in Baghmata river basin, Bihar

R. Vinu Chandran<sup>1</sup>, D. Ramakrishnan<sup>1\*</sup>, V. M. Chowdary<sup>1</sup>, A. Jeyaram<sup>1</sup> and A. M. Jha<sup>2</sup>

<sup>1</sup>Regional Remote Sensing Service Centre, Indian Institute of Technology Campus, Kharagpur 721 302, India

<sup>2</sup>Space Applications Centre, Ahmedabad 380 015, India

**This study pertains to analysis of Airborne Synthetic Aperture Radar (ASAR) images in mapping the flood inundation and causative factors of flood in the lower reaches of Baghmata river basin for the period July–October 2004. Integration of the flood inundation layer and land cover layer derived from LISS III data indicate that 62% of the agricultural area was inundated. Floodwater drained faster in the left bank, whereas it was slow in the right bank. The Digital Elevation Model of the area shows that the flood-prone right bank of the Baghmata river is a topographic low sandwiched between Kosi and Burhi Gandak highs (megafans). The Baghmata river flows at high elevation than the right bank area. Low width-to-depth, high Sa/Se ratios indicate vulnerability for flooding due to low carrying capacity and avulsion. Over-bank flow is observed to initiate from the reactivation of underfit channels and tributaries. The low topography, low carrying capacity and avulsive behaviour of the river are attributed herein to frequent and prolonged flooding of the right**

\*For correspondence. (e-mail: aarkay\_geol@yahoo.com)

**bank. In this particular case, the earthwork along the river course also is found to impede the recession of floodwater.**

**Keywords:** Air-borne synthetic aperture radar, Baghmata river, digital elevation model, flood water.

THE alluvial plains of north Bihar are the most vulnerable for flood hazard. This area is observed to have the highest flood incidences<sup>1</sup>, with a frequency of two years<sup>2</sup>. Floods result in innumerable losses in terms of human lives, livestock and infrastructure<sup>3</sup>. Flood monitoring is a primary issue in the management of resources, especially in situations of emergency, with the need to provide an overall picture of the situation in a short time. Satellite remote sensing has high potential in flood inundation mapping. Optical imageries are used routinely for flood mapping, but may be unavailable during flood season due to cloud cover<sup>4-6</sup>. The unique advantage of radar remote sensing compared to passive sensors is that it can penetrate clouds and hence is helpful to map flood inundation in adverse weather conditions. The Airborne Synthetic Aperture Radar (ASAR) system can obtain significantly high spatial resolution through advanced signal processing and precise pulse compression techniques. However, identification of objects from SAR images is quite difficult as the imaging mechanism is different from the conventional optical sensors, since radar backscatter is a function of the surface roughness and dielectric constants of the imaged area. Interpretation of SAR imageries for flood mapping is done by grey-level thresholding<sup>7</sup>, textural classification and histogram slicing<sup>8</sup>. Textural analysis is commonly used to identify objects and features in a radar image and can aid topography mapping. The deviation changes<sup>9</sup> after textural transformation is taken advantage here in mapping the flood-inundated areas.

The foothills-fed Baghmata river flows through the interfan area between the Gandak and Kosi megafans and finally joins the Kosi river<sup>10</sup>. The Baghmata river basin was extensively investigated from the point of fluvial dynamics, morphometry, avulsive behaviour and sediment characters *vis-à-vis* flood hazard<sup>11-14</sup>. This communication attempts to map and understand causes for flood with a real-time study (during July–October 2004) using ASAR. An attempt is also made to understand the drainage characteristics of Baghmata river *vis-à-vis* frequent flooding.

The investigated area forms the lower reaches of the Baghmata river near its confluence with Kosi river (Figure 1). The area is bound between lat. N25°30'–N25°40' and long. E86°24'–E86°30' that covers 115 km<sup>2</sup>. The average annual rainfall of the catchment area is more than 1200 mm, mostly distributed between June and September. Geologically, the study area comprises alluvial material of Recent to sub-Recent period. The Baghmata river and its environs are also influenced by active sub-surface fault systems<sup>15</sup>. Geomorphologically, this alluvial plain is cha-

racterized by ubiquitous presence of cut-off meanders and underfit channels formed due to frequent river avulsions.

Flood impact assessment was done using temporal ASAR images (C-band) acquired during three periods corresponding to pre-flood (10 June 2004), during flood (22 July 2004) and post-flood (10 October 2004). The landuse/landcover map of the study area was generated using LISS III (December 2002). These imageries were geometrically corrected using SOI toposheets. SOI maps and collateral data were used for identifying different terrain features on the image. Satellite images were then co-registered and processed using ERDAS IMAGINE digital image processing software ver. 8.7. The impact of the flood on landuse of the study area was assessed by integrating the flood inundation layers with the landuse/landcover layer in the GIS (Geographic Information System) environment. Processing of SAR images involves speckle removal and textural classification, which are discussed below.

Presence of speckle in radar imageries degrades the interpretability of the imagery. Speckle in imaging radar is mathematically modelled as multiplicative noise with a mean of 1. Various algorithms are available to suppress the speckle and improve the image quality. For this study, Lee-sigma filter<sup>16</sup> was used for speckle suppression. The Lee-sigma filter assumes that 95.5% of random samples are within a range of  $\pm 2$  standard deviation. It replaces the pixel of interest with the average of all DN values within the moving window that falls within the designated range. Coefficient of variation was computed for each scene separately and a kernel window of  $5 \times 5$  was used to run the filter.

Radar images have their own specific characteristics and are quite different from optical and infrared remote sensing. Image texture is considered as the change and repeat of image grey in space, or local pattern in image and its arrangement rules. Physical properties captured in the image depend on the backscatter of the ground. For the present analysis, enhancement using variance (second order) algorithm was employed. Variance is computed using the eq. (1).

$$\text{Variance} = \frac{\sum(x_{ij} - M)^2}{n - 1}, \quad (1)$$

where  $x_{ij}$  is the DN value of pixel ( $i, j$ ),  $n$  the number of pixels in a window and  $M$  the mean of the moving window, where

$$M = \frac{\sum x_{ij}}{n}.$$

Texture in radar imagery sharply varies with objects. Calm water surface causes specular reflection and appears dark and smooth, whereas ripples may cause variations in the tone. For a totally flooded field, like rivers and water

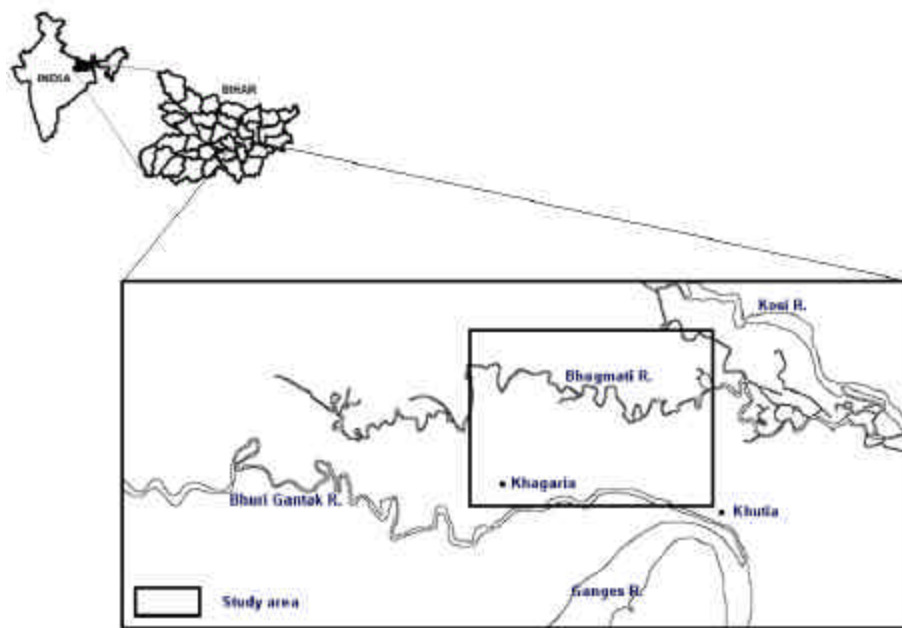


**Figure 1.** Location map of the study area.

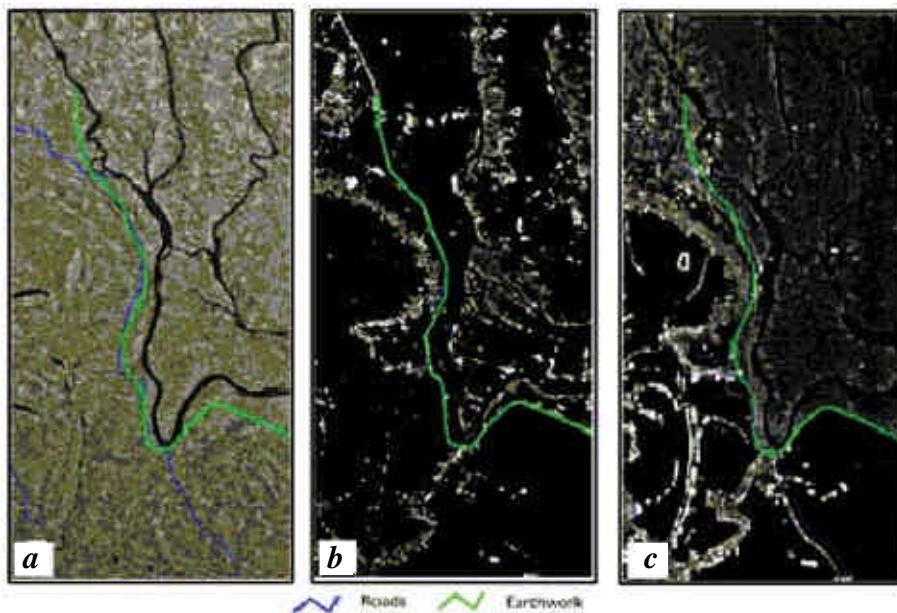


**Figure 2.** Processed ASAR images of the study area: *a*, Pre-flood, June 2004; *b*, Flood July 2004; *c*, Post-flood, October 2004. Black shade represents water.

bodies, the backscattering coefficient ( $S^0$ ) will be low. Vegetated areas yield more complex response as part of the energy is scattered by the canopy and is partly transmitted to the ground. The backscattering coefficient from a flooded vegetated area may then be higher relative to the same area under dry conditions<sup>8</sup>. For textural analysis, a window size of  $11 \times 11$  was used. Though larger window size gives more accurate estimation, it becomes difficult to delineate the boundaries. LISS-III image of the same area was used to generate the landcover map. Flood inun-

ation layer was overlaid over the landcover map to find out the area inundated under each landcover category. Image differencing between the pre-flood and flood events was also carried out to delineate the sites of embankment and riprap failures.

The Shuttle Radar Topographic Mission (SRTM)-derived Digital Elevation Model (DEM) was co-registered with other optical and ASAR databases. The height information derived from DEM was calibrated with spot heights (50 samples) from the topographic sheets using

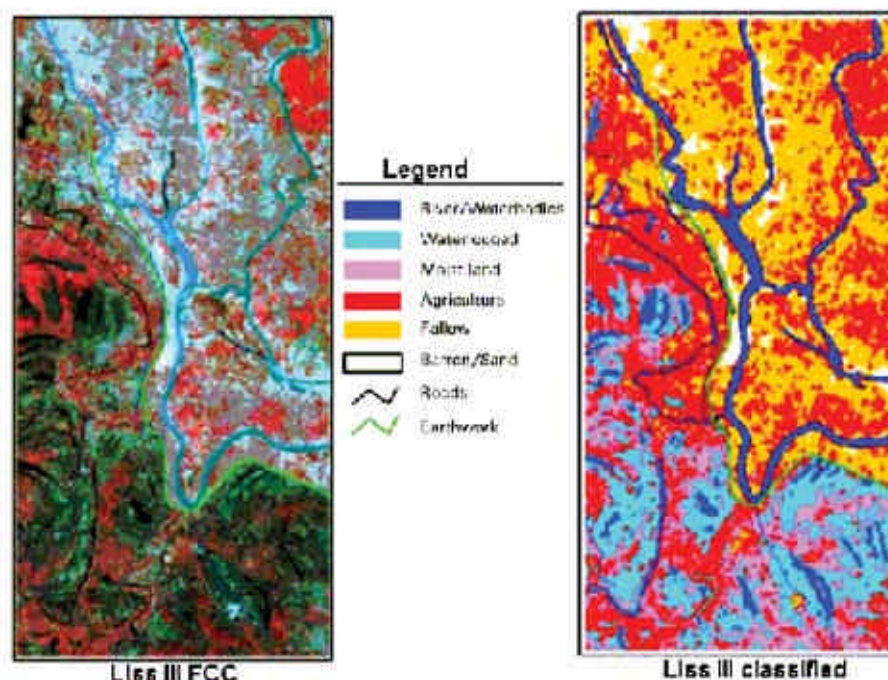


Figure 3. IRS 1D LISS III FCC and classified image of the study area.

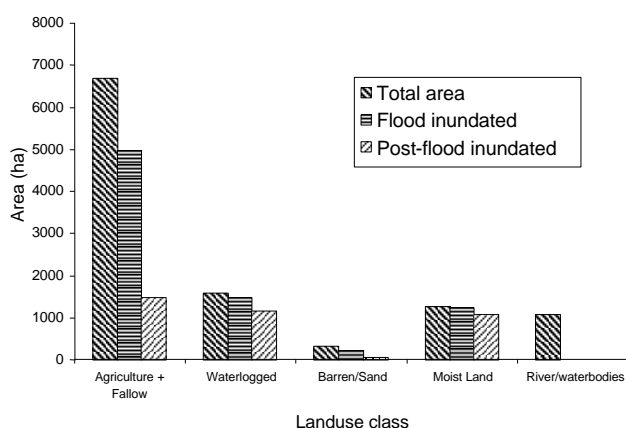


Figure 4. Area under flood inundation for various landcover classes in Khagaria district, Bihar.

second-order polynomial equation (RMS error = 0.5). The DEM thus derived is used herein for analyses on account of higher accuracy over DEM derived from the spot heights.

GIS is a handy tool for spatial analysis of data. Area statistics and vector layer with polygon topology of flood inundation area, and statistics for the pre-flood, flood and post-flood periods were derived from the processed ASAR images using Arc Map ver. 9.0. From the LISS III classified imagery, vector coverage of different landuse classes was derived. By overlay analysis of flood inundation and landcover coverages, statistics of flood inundation area in each land use class was estimated.

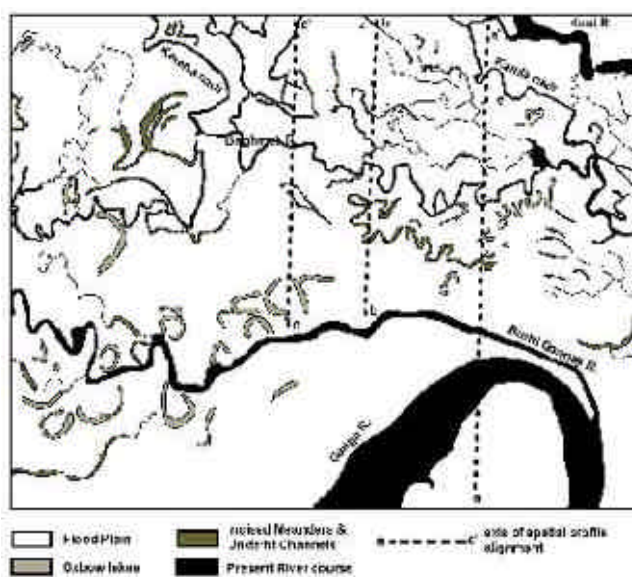
Separate arc coverages of roads and embankment were made for visual analysis and map composition.

Water-spread areas in the three seasons were detected by grey-level threshold of the classified images. Grey-level clusters representing different classes were visually identified and attributed different colours. Processed radar images for pre-flood, during flood and post-flood seasons are shown in Figure 2. In the pre-flood image, it was observed that the major water-spread area is under the river course and waterlogged areas. An area of 1077.2 ha is covered by water during this season. During the flood season, an additional 6797.50 ha is inundated (62% of the total area). During post-flood (October), the water-covered area excluding water bodies is found to be 3369.4 ha. Statistics on the landcover classes (Figure 3), area under water inundation and percentage of total area for each class during flood and post-flood is shown in Table 1 and Figure 4. Area statistics show that 7875 ha (72%) of the study area is inundated during the flood season. Of the cropped area, 73 and 30% is inundated in the flood and post-flood seasons respectively, and more than 85% of the moist land is under flood cover during both the seasons. Interestingly, it is observed that water has receded from the northern portion and low-lying areas during post-flood, but areas south of the earthwork towards the bottom are still under water. We have studied the geomorphology of the area to find out the causes of flooding and differential water retention. Results are discussed below.

Though the Baghmata river drains between the Gandak and Kosi interfan area, it has been active from the historic past till date. The fluvial history of the Baghmata river in

**Table 1.** Total area for each landuse class and area under flood inundation

Land cover class	Total	Inundated area (ha)			
		Flood	Percentage	Post-flood	Percentage
Agriculture + fallow	6693.12	4959.33	74.10	1485.54	22.20
Waterlogged	1585.36	1463.33	92.30	1160.97	73.23
Barren/sand	312.745	225.08	71.97	51.90	16.59
Moist land	1269.44	1226.96	96.65	1081.34	85.18
River/waterbodies	1077.2	–	–	–	–
Total	10937.87	7874.7	–	4446.60	–

**Figure 5.** Fluvial geomorphology of the study area.

the past 230 years envisaged at least eight major avulsions (besides several minor avulsions), each amounting to 5 to 6 km lateral shift in drainage course<sup>10,12</sup>. This is best reflected in the LISS III image by way of anabranching, multichannel drainage system (Figure 5). The frequent drainage avulsions resulted in the development of several underfit channels and cut-off meanders. It is evident from the pre- and post-flood ASAR images that these underfit channels play a significant role during floods by way of reactivation (Figure 6).

The channel morphological parameters (width–depth ratio, sinuosity, braid–channel ratio), hydrological factors (peak discharge, sediment load) and terrain characteristics (gradient) play a significant role in over-bank flow<sup>2,17</sup>. In the study area channel morphology is characterized by a typical width–depth (w/d) ratio ranging from 6 (near Amba village) to 30 (near Narandih village downstream of Kareha and Kachna nadi confluence). The sinuosity varies between 2.8 (near Mohanpur village) and 3.5 (near Kudra village). Thus, the w/d ratio at downstream reaches of Baghmata river is considerably lower than that in the upper

reaches. These factors tend to lower the carrying capacity of the river during periods of high discharge. Further, in the Baghmata basin, the peak discharge in the downstream reaches tends to be higher than the upstream reaches. Thus, the lower reaches of Baghmata river are more vulnerable to over-bank flow.

The spatial profiles (transverse and longitudinal) of the Baghmata river and its tributaries (Figures 7 and 8) derived from the DEM indicate the following points:

- The Baghmata river flows through a topographic low sandwiched between Kosi and Gandak megafans.
- Even within the Baghmata basin, the left bank is elevated compared to the right bank.
- The Baghmata river occupies a topographically elevated area than the right bank.
- Since the topography is low, the underfit channels and tributaries of the right bank are reactivated and act as conduits for surplus water during high discharge periods.

The Sa/Se ratio<sup>18,19</sup> between the gradient of potential avulsive course (Sa) and gradient of existing channel (Se) was computed from the DEM. It varies from 0.75 to 1.0. This again points to the tendency of river avulsion in the right bank area. Thus, the right bank of the Baghmata in the downstream reaches is more vulnerable to flooding by virtue of its low topography, channel morphology and high peak discharge. Flood vulnerability of the right bank is best exemplified during the 2004 flood event. Image differencing between the pre-flood and flood ASAR images indicates that:

- During the flood event, tributaries are buffered by dark tone and smooth textured area, whereas in regions away from the tributaries the tone is light and texture is rough (Figure 6b). This implies that there is a reduction in energy received at the sensor all along the length of these channels. This observation is attributed to change in the reflection due to increased water column depth near the tributaries. Thus, the interconnected minor shallow channels are responsible for the overland flow, which could not cope up with the high discharge rate.

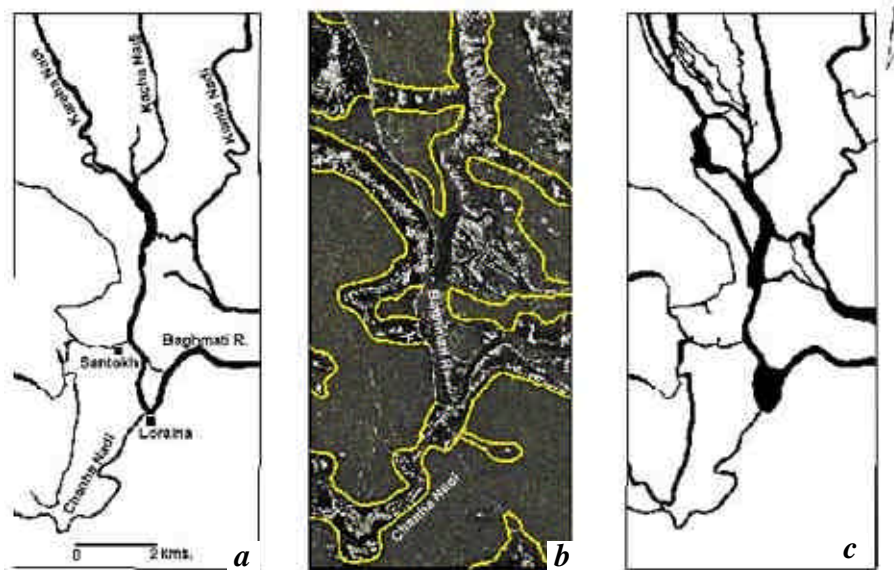


Figure 6. Drainage configuration of Baghmata river during (a) pre-flood, (b) flood and (c) post-flood.

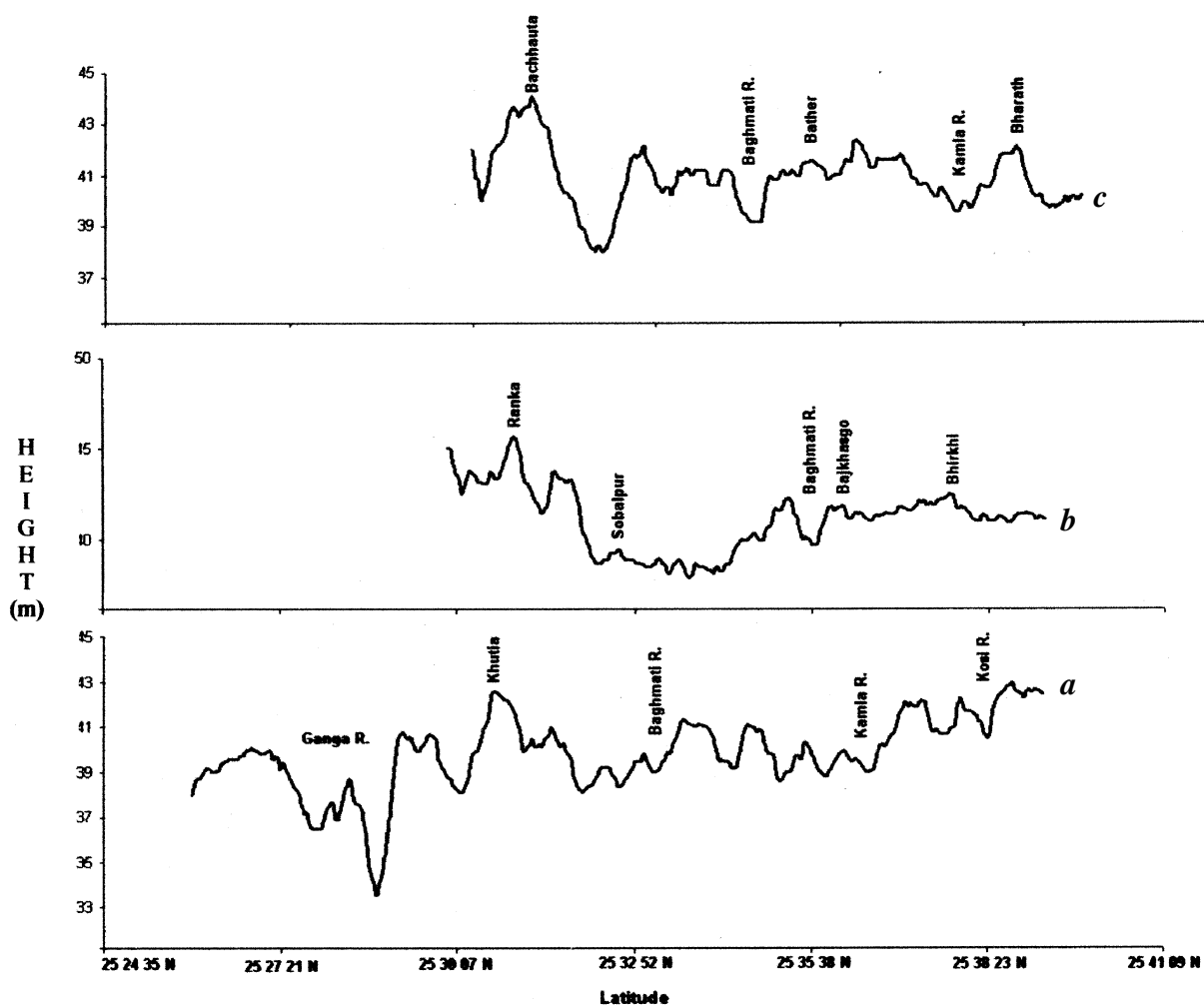


Figure 7. Transverse spatial profiles across (a) Kosi-Ganga transect, (b) Bhirkhi-Ranka transect and (c) Bharath-Bachhauta transect along longitudes 86 32 56E, 86 27 58E and 86 30 19E respectively.

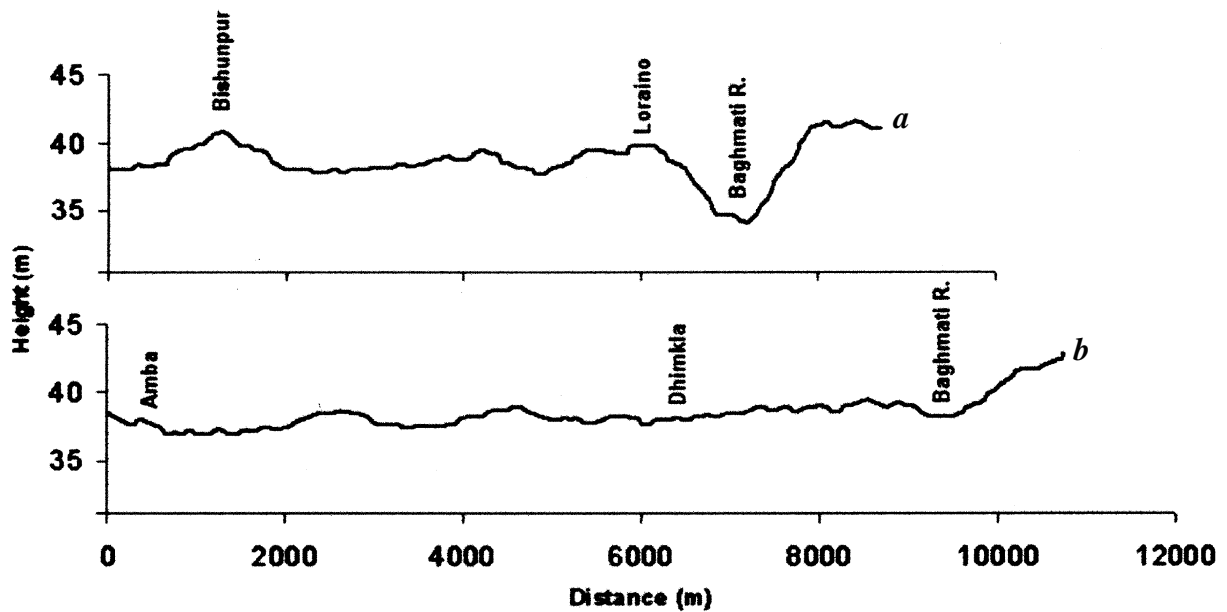


Figure 8. Longitudinal spatial profiles along (a) Chanha nadi and (b) underfit channel of Baghmata.

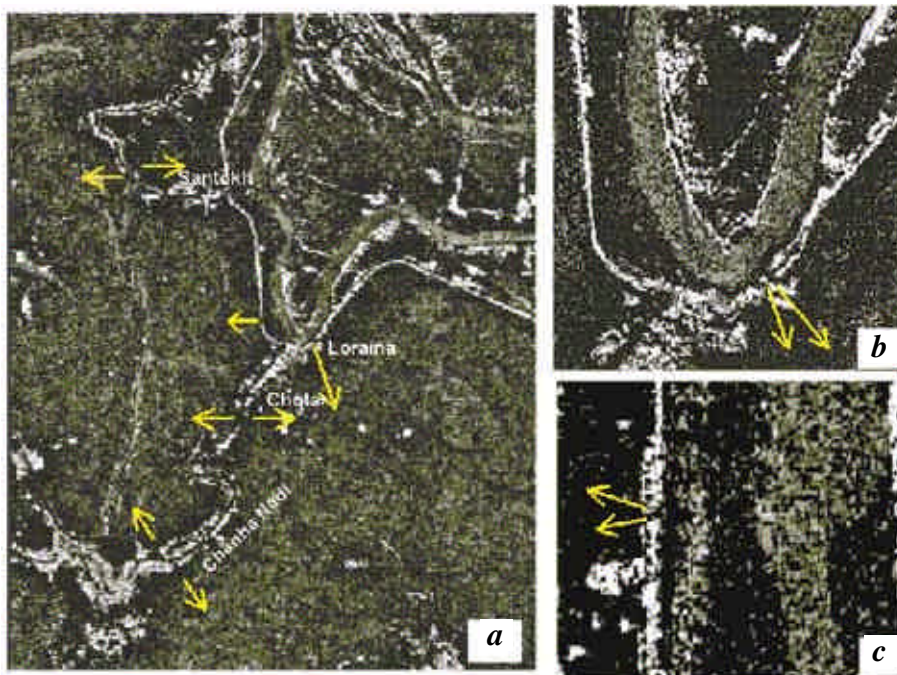


Figure 9. Difference image (pre-post) showing flooding from tributaries (a) and embankment failure (b, c).

(ii) Similar changes in texture and tone were also observed in areas adjacent to embankment failure along the Baghmata river, indicating flooding on account of structural failures (Figure 9). These failures are distinctly seen near the villages of Loraina, Dahma, southeast of Santokh, Marukah and Chharra Patti.

As mentioned earlier, floodwater drained faster in the area between the rivers Baghmata and Kosi. At the same time, between Baghmata and Burhi Gandak, floodwater drainage is slow. The study area is characterized by low topography with marshy and wetlands as seen in the LISS III classified image (Figure 3). Since Baghmata river is

the only outlet for draining the floodwater, drainage through these channels is possible only when the discharge of Baghmata river returns to normal. Under these conditions, the embankment constructed along the right bank of Baghmata river acts as a barrier and retards faster draining of water to the Baghmata river.

ASAR images are useful for flood inundation mapping when conventional optical data are not available due to cloud cover. High spatial resolution of ASAR images coupled with optical data help in assessing the extent of damage to agriculture and basic infrastructure. In the present study, it is observed that the right bank of the Baghmata river undergoes frequent flooding due to topography, channel morphometry and discharge characters. Reactivation of underfit and tributary channels seems to initiate overland flow in the low-land. Failure of embankment, particularly along river meanders adds to the severity. Since Baghmata flows at a higher elevation, the floodwater retreat in the southern bank is possible only after normal discharge in the Baghmata river. Thus, the embankment constructed along the course (Baghmata and Burhi Gantak) is found to impede the recession of floodwater.

1. Kale, V. S., Flood studies in India: A brief review. *J. Geol. Soc. India*, 1997, **49**, 359–370.
2. Sinha, R. and Jain, V., Flood hazards in north Bihar rivers, Indo-Gangetic plains. *J. Geol. Soc. India*, **41**, 27–52.
3. Jain, V. and Sinha, R., Evaluation of geomorphic control on flood hazard through Geomorphic Instantaneous Unit Hydrograph. *Curr. Sci.*, 2003, **85**, 1596–1600.
4. Giacomelli, A., Mancini, M. and Rosso, R., Assessment of flooded areas from ERS-1 PRI data: An application to the 1994 flood in northern Italy. *Phys. Chem. Earth*, 1995, **20**, 469–474.
5. Du, L. J., Texture segmentation of SAR images using localized spatial filtering. International Geoscience and Remote Sensing Symposium, 1990, vol. 4, pp. 1983–1986.
6. Wang, Y., Koopmans, B. N. and Pohl, C., The 1995 flood in the Netherlands monitored from space – a multi sensor approach. *Int. J. Remote Sensing*, 1995, **16**, 2735–2739.
7. Laws, K., Goal-directed texture-image segmentation. *SPIE-Appl. Artif. Intell.*, 1985, **548**, 19–26.
8. Ormsby, J. P., Blanchard, B. J. and Blanchard, A. J., Detection of low land flooding using active microwave systems. *Photogramm. Eng. Remote Sensing*, 1985, **51**, 317–328.
9. Lee, J. H. and Philpot, W. D., Spectral texture matching: A classifier for digital imagery. *IEEE Trans. Geoscience Remote Sensing*, 1991, **29**, 545–554.
10. Jain, V. and Sinha, R., Fluvial dynamics of an anabranching river system in Himalayan foreland basin, Baghmata river, north Bihar plains, India. *Geomorphology*, 2004, **60**, 147–170.
11. Sinha, R., Channel avulsion and flood plain structure in the Ganak–Kosi interfan, north Bihar plains, India. *Z. Geomorphol.*, 1996, 249–268.
12. Jain, V. and Sinha, R., Derivation of unit hydrographs from GIUH analysis for a Himalayan river. *Water Resour. Manage.*, 2003, **17**, 355–375.
13. Jain, V. and Sinha, R., Hyperevulsive-anabranching Baghmata river system, north Bihar plains, eastern India. *Z. Geomorphol.*, 2003, **47**, 101–116.
14. Sinha, R., Gibling, M. R., Jain, V. and Tandon, S. K., Sedimentology and avulsion patterns of the anabranching Baghmata river in the Himalayan foreland basin, India. *Spec. Publ. Int. Assoc. Sedimentol.*, 2005, **35**, 181–196.
15. Dasgupta, S., Tectono-geologic framework of eastern Gangetic foredeep. *J. Geol. Soc. India*, 1993, **31**, 61–69.
16. Lee, J. S., Speckle analysis and smoothing of synthetic aperture radar images. *Comput. Graphics Image Process.*, 1981, **17**, 24–32.
17. Sinha, R. and Friend, P. F., River systems and their sediment flux, Indo-Gangetic plains, northern Bihar, India. *Sedimentology*, 1994, **41**, 825–845.
18. Jones, L. S. and Harper, J. T., Channel avulsions and related processes, and large-scale sedimentation patterns since 1875, Rio Grande, San Luis Valley, Colorado. *Geol. Soc. Am. Bull.*, 1998, **110**, 411–421.
19. Jones, L. S. and Schumm, S. A., Causes of avulsion: an overview. In *Fluvial Sedimentology VI* (eds Smith, N. D. and Rogers, J.), International Association of Sedimentologists Special Publication 28, Blackwell Science, Oxford, 1999, pp. 171–178.

Received 14 March 2005; revised accepted 19 November 2005